Space Sciences Laboratory Series 11, Issue 75

Final Report

for

Energetic Particle Flux Experiment (AIMP-D & E)

(28 January 1965 to 31 October 1969)

Contract No.: NAS 5-9077

Prepared by

Space Sciences Laboratory
University of California
Berkeley, California 94720

Principal Investigator: K.A. Anderson

for

Goddard Space Flight Center
Greenbelt, Maryland

Space Sciences Laboratory Series 11, Issue 75

Final Report

for

Energetic Particle Flux Experiment (AIMP-D & E)

(28 January 1965 to 31 October 1969)

Contract No.: NAS 5-9077

Prepared by

Space Sciences Laboratory
University of California
Berkeley, California 94720

Principal Investigator: K.A. Anderson

for

Goddard Space Flight Center
Greenbelt, Maryland

TABLE OF CONTENTS

ABSTRACT

This report summarizes the scientific usage of the data from the University of California experiments aboard Explorer 33 and 35 (AIMP-1 and 2). Basically, three major fields of study have been pursued in the analysis of the data. These are energetic solar particles in the interplanetary medium, terrestrial particle fluxes in the magnetotail and magnetosheath-bow shock regions, and lunar effects on energetic particles. Much of the work on solar particle studies is based on comparisons with simultaneous observations on other spacecraft (IMP-3, OGO-1 and -3, OGO-5, IMP-4 and -5) as well as with ground-based optical and radio observations.

Studies of terrestrial fluxes have concentrated on the "island" fluxes, the distant ($\sim$60 R_e) magnetotail, and the magnetosheath and bow shock spikes which are observed even $\sim$60 R_e upstream from the earth in the interplanetary medium.

Lunar particle shadow studies, utilizing both solar and terrestrial particles, have proven to be very fruitful in delineating the structure and dynamics of the magnetosphere. Work is continuing on energetic particle interactions with the moon.

Much of the work on this contract has been done by students. Part of the PhD thesis of Dr. Robert P. Lin was based on Explorer-33 data. Dr. S.W. Kahler also participated in joint OGO-1 and -3 and Explorer-33 and 35 studies of solar events as part of his graduate work. R.E. McGuire, currently a graduate student, is involved with continuing work on lunar particle shadows. He has recently completed a theoretical study of particle shadows based on the observations of of Explorer-35.

A substantial amount of work has been done and is continuing to be done in collaboration with other experimenters on these same spacecraft as well as with experimenters on other spacecraft. Much analysis remains to be done on the Explorer-35 data.

All of the Explorer-33 and the first year of Explorer-35 data has been edited and submitted to the National Space Science Data Center.

The rest of the report consists of the following:

I. Technical Description of the University of California experiments on Explorer 33 and 35.

II. A Description of the Data Tape Format.

III. A summary of the computer programs developed to process the data for the University of California experiments.

IV. A bibliography of the articles published or submitted for publication that are based on data from these experiments and a list of papers given at scientific meetings which are based on data from Explorer 33 and 35.

LIST OF ILLUSTRATIONS

I. TECHNICAL DESCRIPTION OF EXPERIMENTS

The University of California experiments aboard Explorer-33 and -35 each contain two Geiger-Mueller tubes, one of which looks directly at particle fluxes while the other observes the particle flux backscattered off an 8 mil gold foil. Protons lose energy in the gold foil without backscattering while electrons backscatter with high efficiency and little energy loss. With this arrangement, proton and electron fluxes can be identified and separated.

In Explorer-33 the open counter, GM2, and the scatter detector, GM1, are both pointing at 90^{o} to the spin axis while in Explorer-35 both detectors point along the spin axis. GM1 is a Lionel 205 HT Geiger-Mueller tube with a standard thickness mica window while GM2 is a thin-window version of the same tube with an energy threshold of about one-half as high as for GM1. Thus for electrons it is possible to derive some energy spectrum information about the fluxes. A 4-inch ionization chamber completes the detector complement which is shown in Figure 1. Table 1 summarizes the characteristics of the detectors.

Geiger-Mueller Detectors

The Lionel 205 HT Geiger Mueller detector has a cylindrical cathode of $\frac{1}{4}$" inside diameter, and it is sensitive to radiation over the entire $\frac{1}{4}$" diameter window. This tube has a 1.2-1.4 mg/cm^2 mica window, and a typical electron detection efficiency versus electron energy curve is shown in Figure 2. The threshold, arbitrarily defined as the 1/e efficiency point, is about 40 keV for these tubes. GM2 is a special thin-window (0.7 mg/cm^2 mica) modified Lionel 205 HT. The window diameter has been necked down to 0.17" in

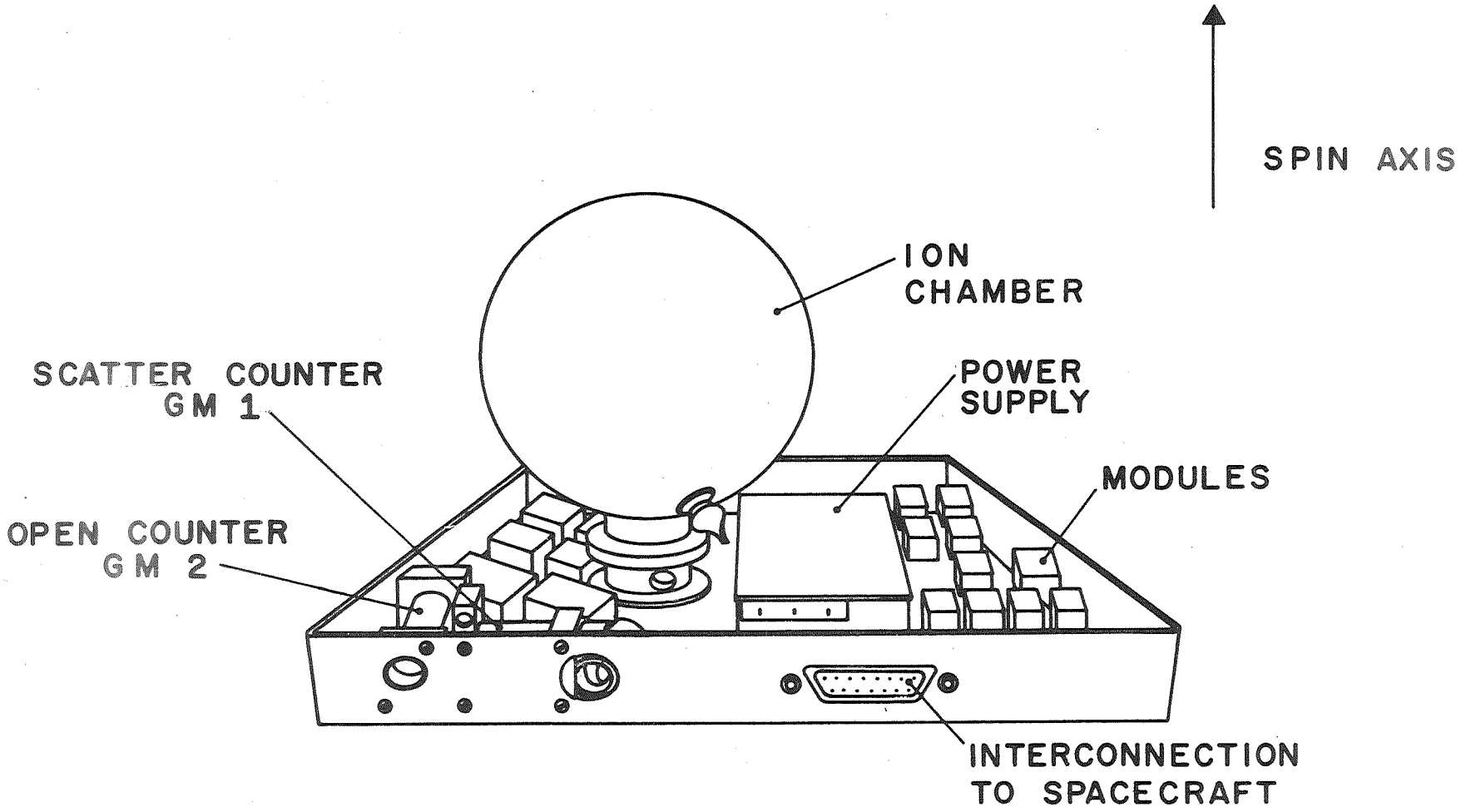

UNIVERSITY OF CALIFORNIA EXPERIMENT PACKAGE FOR EXPLORER 33

Figure 1

Table 1

EXPLORER 33 AND 35 DETECTOR CHARACTERISTICS

Detector Designation	Type of Detector	Window	Directional Sensitivity		Omnidirectional Sensitivity		Geometry Factor		Look Angle FWHM	Angle to Spin Axis
			Electrons	Protons	Electrons	Protons	Directional cm^2-ster	Omni-directional cm^2		
GM1	Lionel 205 HT GM tube in scatter configuration	1.4 mg/cm^2 mica	> 45 keV	None	> 4 MeV	> 40 MeV	2.4×10^{-2} on 33 (3.6×10^{-2} on 35)	~0.75	~60°	90° on 33 (20° on 35)
GM2	Lionel 205 HT thin window GM tube	0.7 mg/cm^2 mica	> 22 keV	> 0.3 MeV	> 4 MeV	> 40 MeV	0.29	~0.75	~75°	90° on 33 (0° on 35)
Ion Chamber	4" diameter spherical Neher-type integrating ion chamber	210 mg/cm^2 aluminum skin	---	---	> 0.7 MeV	> 12 MeV Maximum sensitivity ~17 MeV	---	~80	---	---

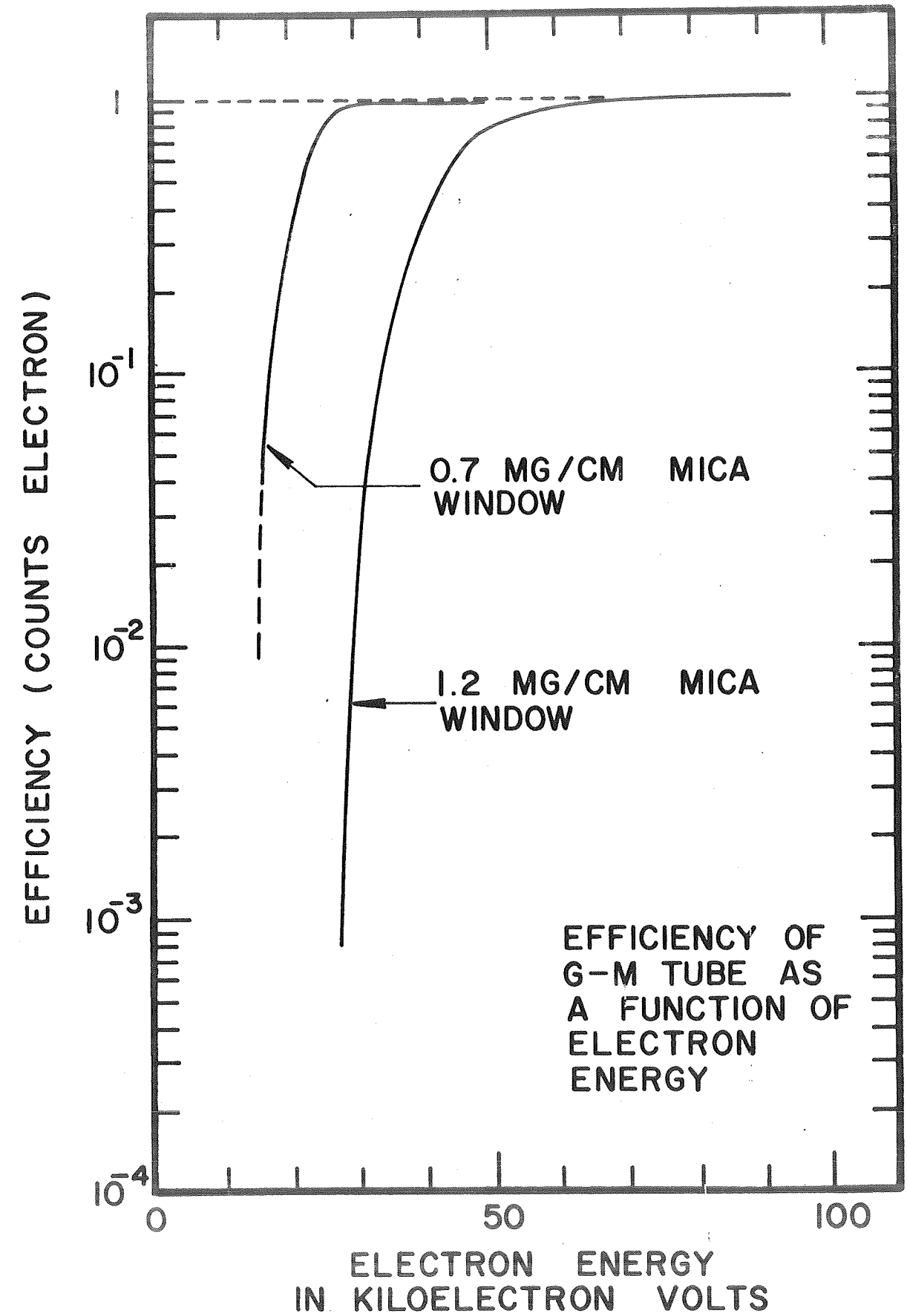
EFFICIENCY (COUNTS ELECTRON)
1
10^{-1}
10^{-2}
10^{-3}
10^{-4}
0.7 MG/CM MICA WINDOW
1.2 MG/CM MICA WINDOW
EFFICIENCY OF G-M TUBE AS A FUNCTION OF ELECTRON ENERGY
0
50
100
ELECTRON ENERGY IN KILOELECTRON VOLTS

Figure 2

order to support the mica window against pressure. Its response to electrons is also shown in Figure 2. As can be seen, its threshold is about 22 keV for electrons.

The proton response of these tubes is calculated from range energy curves given by Trower[1] after the tube window thicknesses are calibrated with an alpha-particle source.

The 8 mil gold scatter foil used in GM1 provides effective discrimination against protons. All particles seen by the counter must backscatter off the foil. Protons lose energy before they are scattered through large angles, as can be illustrated by calculating the rms scattering of a 10 MeV proton in a length equal to its range. From Fermi:[2]

$$\overline{\theta^2} \approx \frac{8\pi N D z^2 Z^2 e^4}{V^2 p^2} \ln \frac{a_o V p}{2 Z^{4/3} z e^2}$$

where N = number of atoms per cm^3, D = length of travel (placed equal to the range), z = charge of particle = 1 for proton, Z = charge of scatter = 79 for gold, e = electron charge, V = velocity of particle, p = momentum of particle, and a_o = Bohr radius. We obtain

$$\sqrt{\overline{\theta^2}} \approx 0.2 \text{ radians} \approx 10^o$$

Tests on the efficacy of the scatter foil for proton rejection were conducted using a cyclotron beam of 4 MeV protons.[3] An upper limit of 0.1% was obtained for the proton detection efficiency. Furthermore the observation of solar proton events in space has confirmed that the count rate of the scatter counter due to backscattered protons is negligible.

Electrons backscatter off the gold foil with high efficiency. A well referenced treatment of electron scattering is contained in Siegbahn,[4] and only the pertinent results will be mentioned here. The 8 mil gold foil is thick enough to insure saturation backscattering of electrons of a few MeV or lower energies. Fifty per cent of a normally incident beam of electrons and 70% of a diffuse beam will be backscattered from the gold foil. The angular distribution of the backscattered electrons will be approximately $\cos^2\theta$ in angular dependence. Neither the backscatter efficiency nor the angular distribution of the backscattered electrons is dependent on the energy of the incident electron. However, energy loss occurs in the scattering foil. Measurements indicate that for a heavy element such as gold the probable energy loss is about 5-10%, with about two-thirds of the particles losing less than 20% of their energy. The effect of this energy loss is two-fold:

1. The energy threshold of the scatter counters are about 5 keV higher than the bare GM tube, and
2. the counting efficiency versus electron energy curve is not quite as sharply falling.

Thus the scatter counter's (GM1) threshold is about 45 keV for electrons. From the above considerations the scattering efficiency would be expected to stay fairly constant over a wide range of electron energy above the threshold for the scatter counter. Figure 3 shows the measured efficiency versus energy for the IMP-3 scatter counter configuration,[3] which is similar to the GM1 detectors flown here.

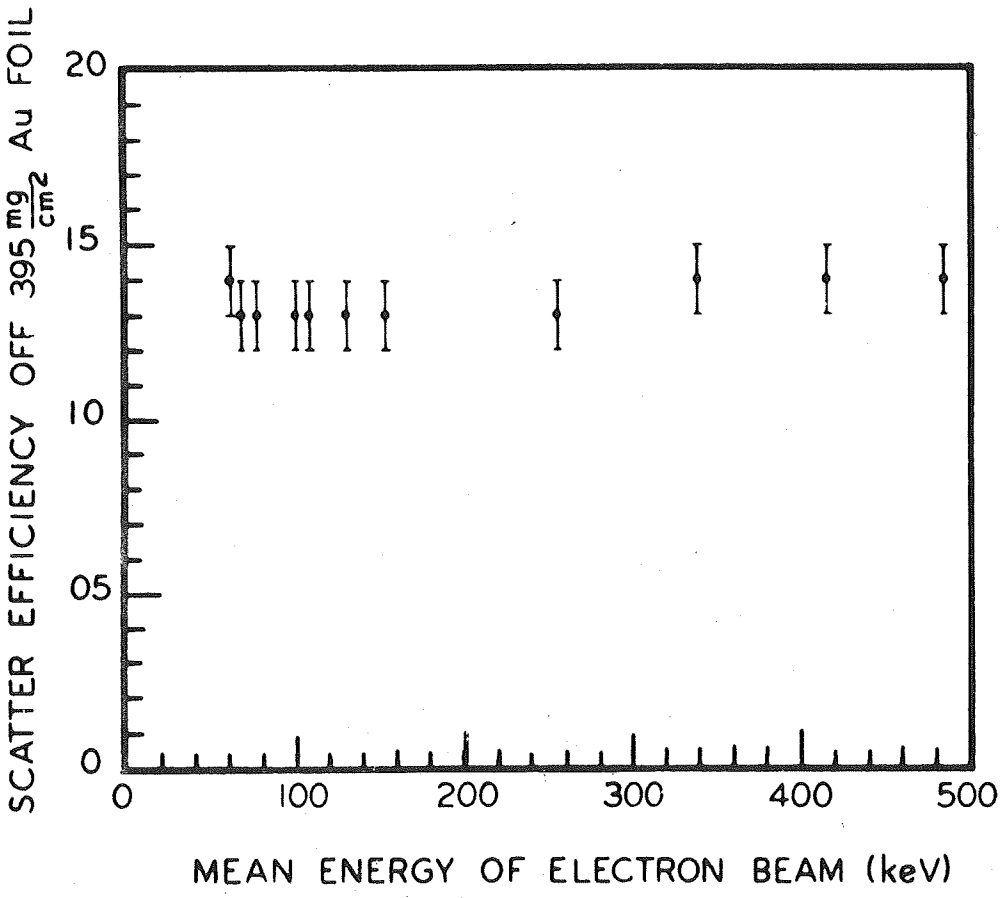

IMP I, II, III GM I SCATTER
COUNTER CONFIGURATION

Figure 3

On Explorer-33, GM2 is pointed at right angles to the spin axis and the spin axis is pointed only 4^{o} off the ecliptic plane. The initial orientation of the spin axis just barely allows GM2 to see the sun; however, as the spin axis-sun angle changes due to the orbital motion of the earth, GM2 sees more and more of the sun. Because of its very thin window GM2 is quite sensitive to solar x-rays in the 1-14$\mathring{A}$ region, and its background count rate is due primarily to such x-rays.

The x-ray response of these counters can be calculated if the composition of the mica window and the fill gas is known. If an x-ray beam of intensity $I_o(\lambda)$ is incident on a material of thickness, ℓ, then the intensity of the penetrating beam is

$$I(\lambda) = I_o(\lambda) \exp [- \rho \ell \sigma (\lambda)]$$

where ρ = density of the material, and $\sigma(\lambda)$ = cross-section.

$$\sigma(\lambda) = \frac{1}{\rho} \sum_i \rho_i \sigma_i (\lambda)$$

where ρ_i = density of element i in the material and $\sigma_i(\lambda)$ = cross-section for element i.

For an x-ray to be counted by the Geiger-Mueller tube, it must penetrate the window and stop in the gas. Therefore, the counting efficiency is given by

$$\frac{I(\lambda)}{I_o(\lambda)} = \exp [- \rho \ell \sigma (\lambda)]_{mica} \langle 1 - \exp [- \rho \ell \sigma (\lambda)]_{gas} \rangle$$

Using the cross-sections kindly supplied by L. Acton (private communication), the calculation has been carried for GM2 of Explorer-33. The resulting efficiency curve is shown in Figure 4.

The detectors on Explorer-35 point along the spin axis which is oriented perpendicular to the ecliptic plane so that no solar x-rays are counted by them. The GM tubes are shielded with 1.5 g/cm^2 of brass. This shielding is in addition to the spacecraft packaging and outer skin so that the total shielding is about 2.0 g/cm^2. Range-energy curves were used to determine the threshold energies for penetrating particles.[1]

The Geiger-Mueller tubes have dead times following a pulse. These dead times change at very high count rates since the voltage across the tube never recovers completely after a pulse before a new pulse starts. The variation of the count rate with flux is shown in Figure 5 for GM1 of the Explorer-33. The assumption of a constant dead time fits the curve well over the tube's useful dynamic range, and individually fitted dead times are used to correct the count rates of the detectors. These are entered as constants in the data processing format (Section II) and are typically $\sim 10^{-4}$ seconds.

The GM detectors have a FWHM opening angle of $\sim 70^{\circ}$. On Explorer-33 the detector points 90° to the spin axis so the count rate is an average over a large cone of angles. In most applications, the GM data is treated as an omnidirectional average.

Ionization Chamber

A schematic of the ion chamber carried aboard Explorer-33 is shown in Figure 6. This is an integrating Neher-type ionization chamber. The operation of the chamber is straightforward. The tungsten whisker flicks over and charges the anode to 700 volts.

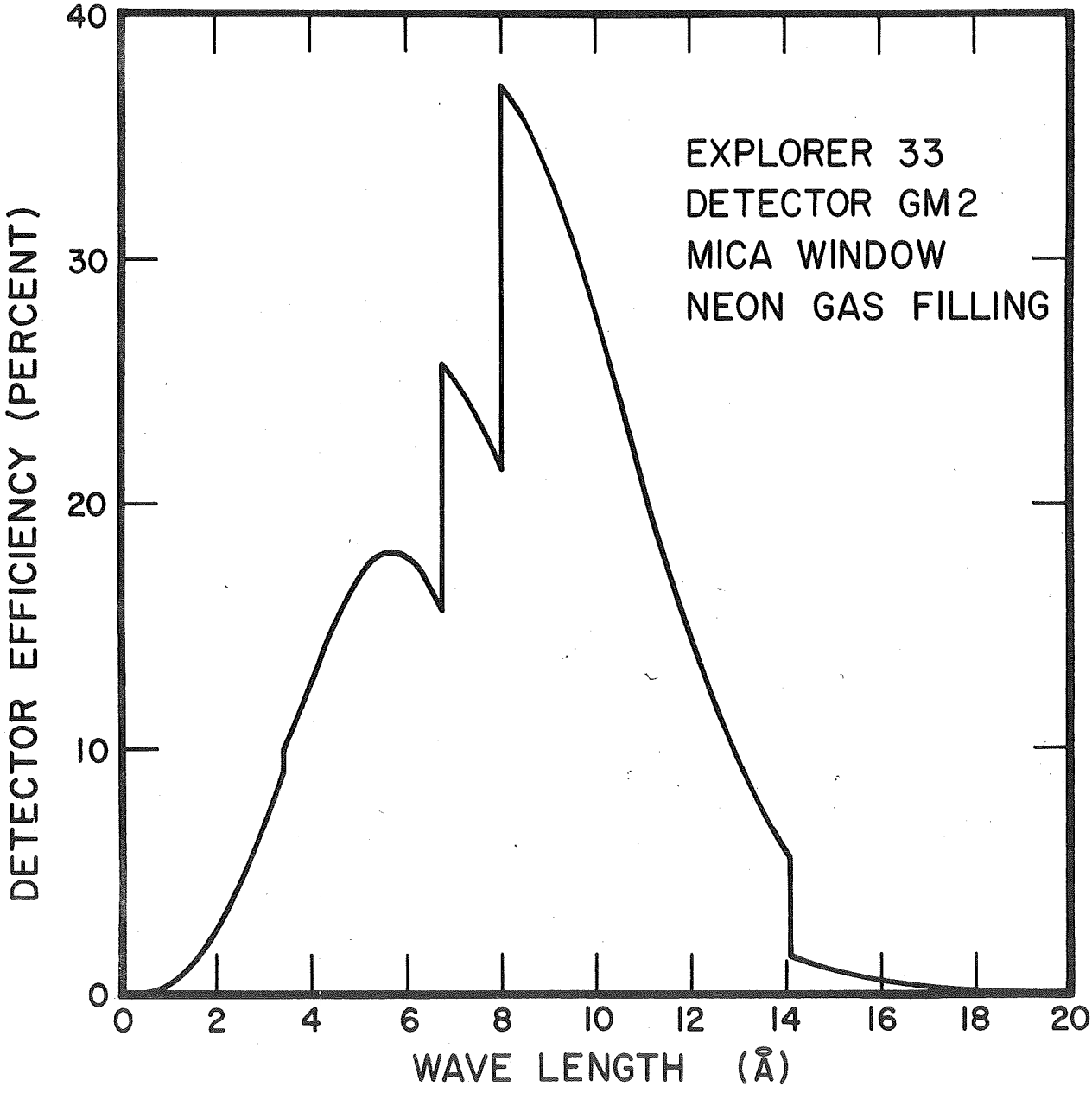
EXPLORER 33
DETECTOR GM2
MICA WINDOW
NEON GAS FILLING
DETECTOR EFFICIENCY (PERCENT)
WAVE LENGTH (Å)
0
10
20
30
40
0
2
4
6
8
10
12
14
16
18
20

Figure 4

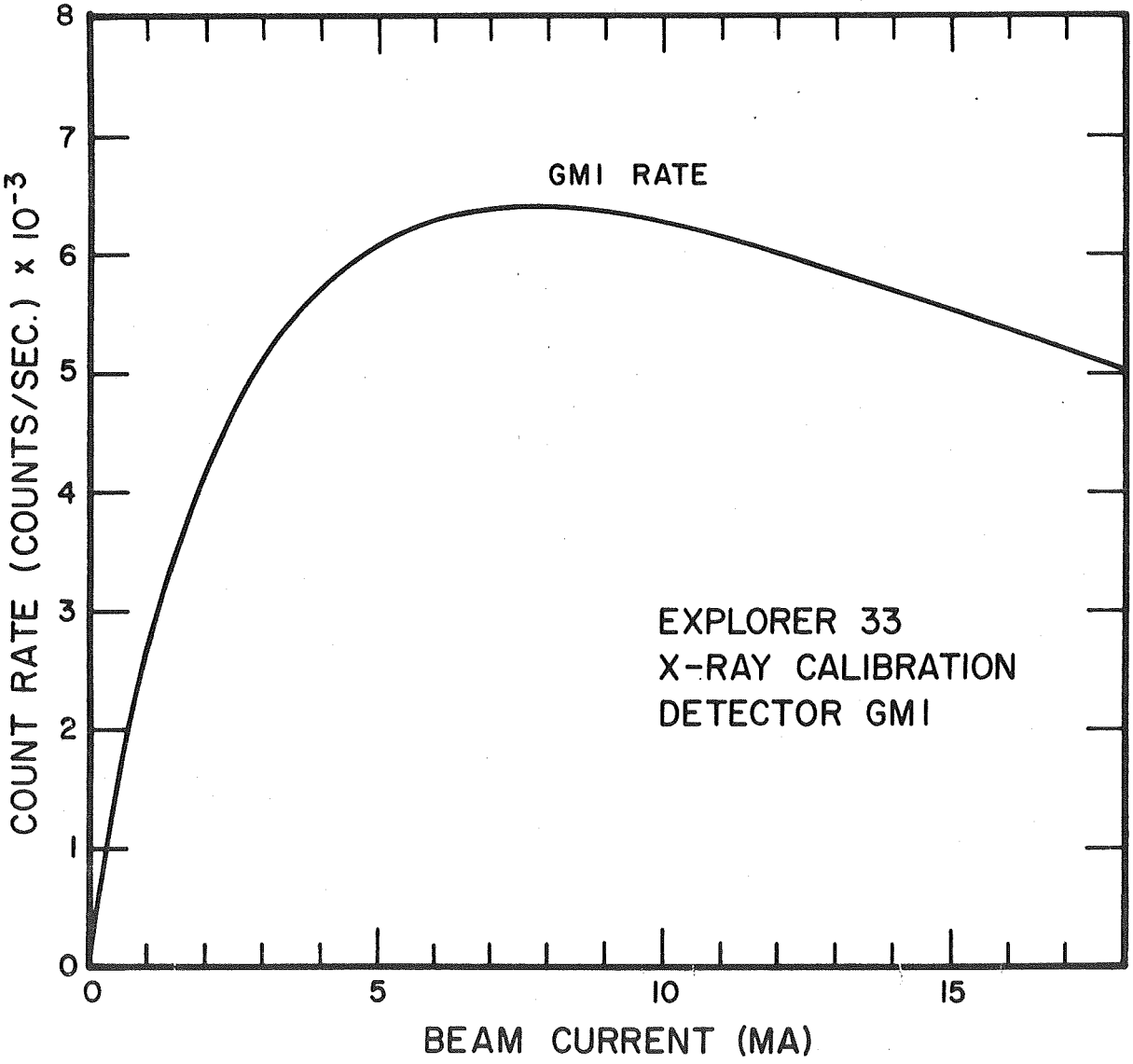
GMI RATE
EXPLORER 33
X-RAY CALIBRATION
DETECTOR GMI
COUNT RATE (COUNTS/SEC.) x 10⁻³
BEAM CURRENT (MA)
0
1
2
3
4
5
6
7
8
0
5
10
15

Figure 5

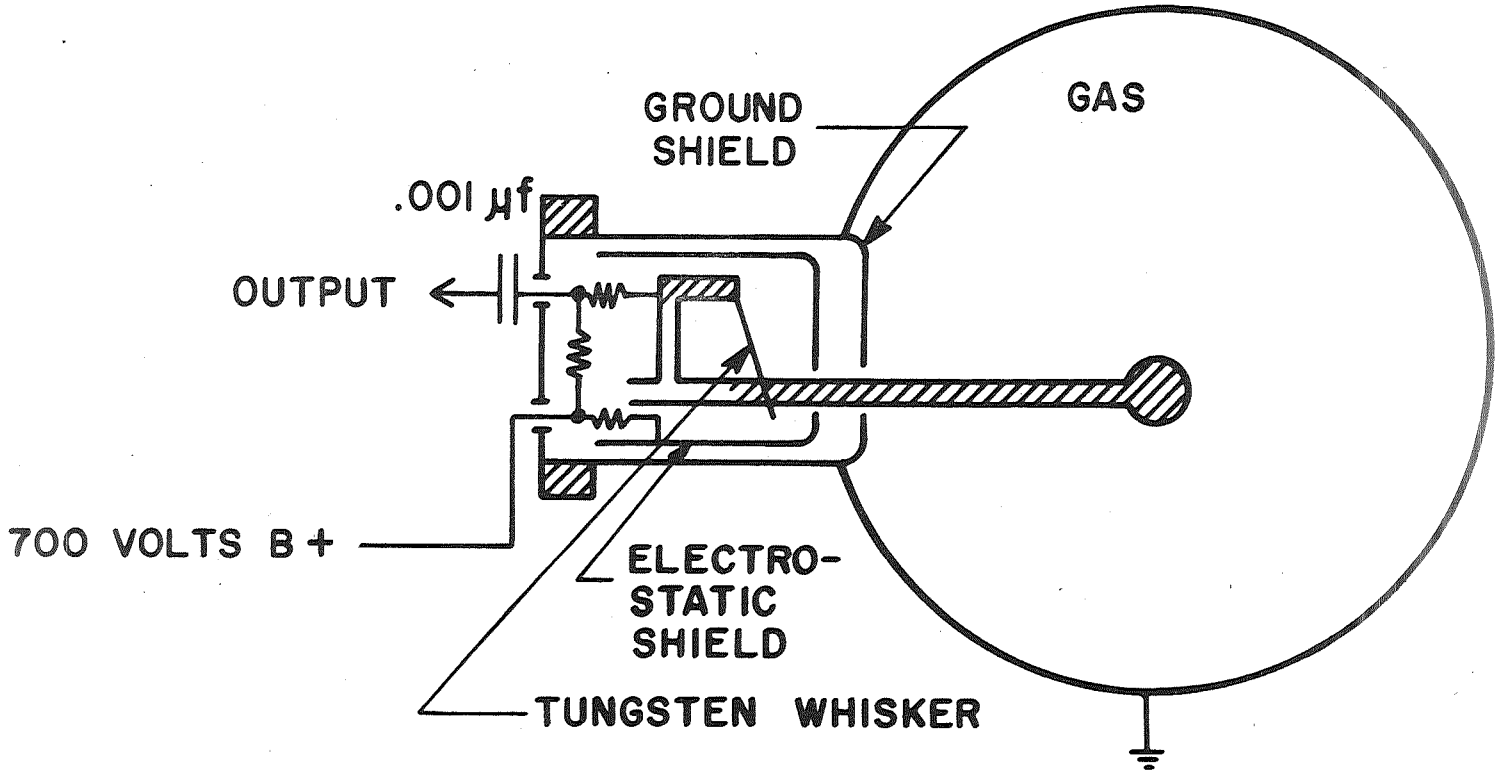

SCHEMATIC, 4" ION CHAMBER

Figure 6

Then the anode collects electrons from ionization in the chamber, making the anode voltage drop. When the drop in anode voltage creates a powerful enough electrostatic force on the whisker, the whisker flicks over and recharges the anode. The pulse created by the recharging is recorded and represents a specific amount of ionization in the chamber. The calibration curves of the Explorer-33 and 35 chambers are shown in Figure 7.

The response of the chamber to protons and electrons of different energies can be calculated. For very high energy (minimum ionizing) particles which penetrate the spacecraft the calculation is fairly simple. However, for low energy particles both the thickness of material surrounding the chamber, and the varying ionization loss of the particle with energy must be taken into account. The amount of energy lost in the chamber can be calculated from range-energy curves, and the material to be traversed before entering the chamber may be estimated from considerations of the ion chamber location on the spacecraft. Figure 8 gives the results of such calculations.

For the Explorer-33 and 35 ion chambers the time span between pulses is measured to milliseconds and read out every 40.96 seconds. Thus the time resolution of the Explorer-33 and 35 ion chambers is an inverse function of the radiation level. At galactic cosmic ray background levels the time resolution is about ten minutes.

Data Handling Electronics

The data from the detector is fed to one 12-bit and three 16-bit accumulators in the digital data processor of the spacecraft encoder after appropriate amplification, shaping and timing. All accumulators

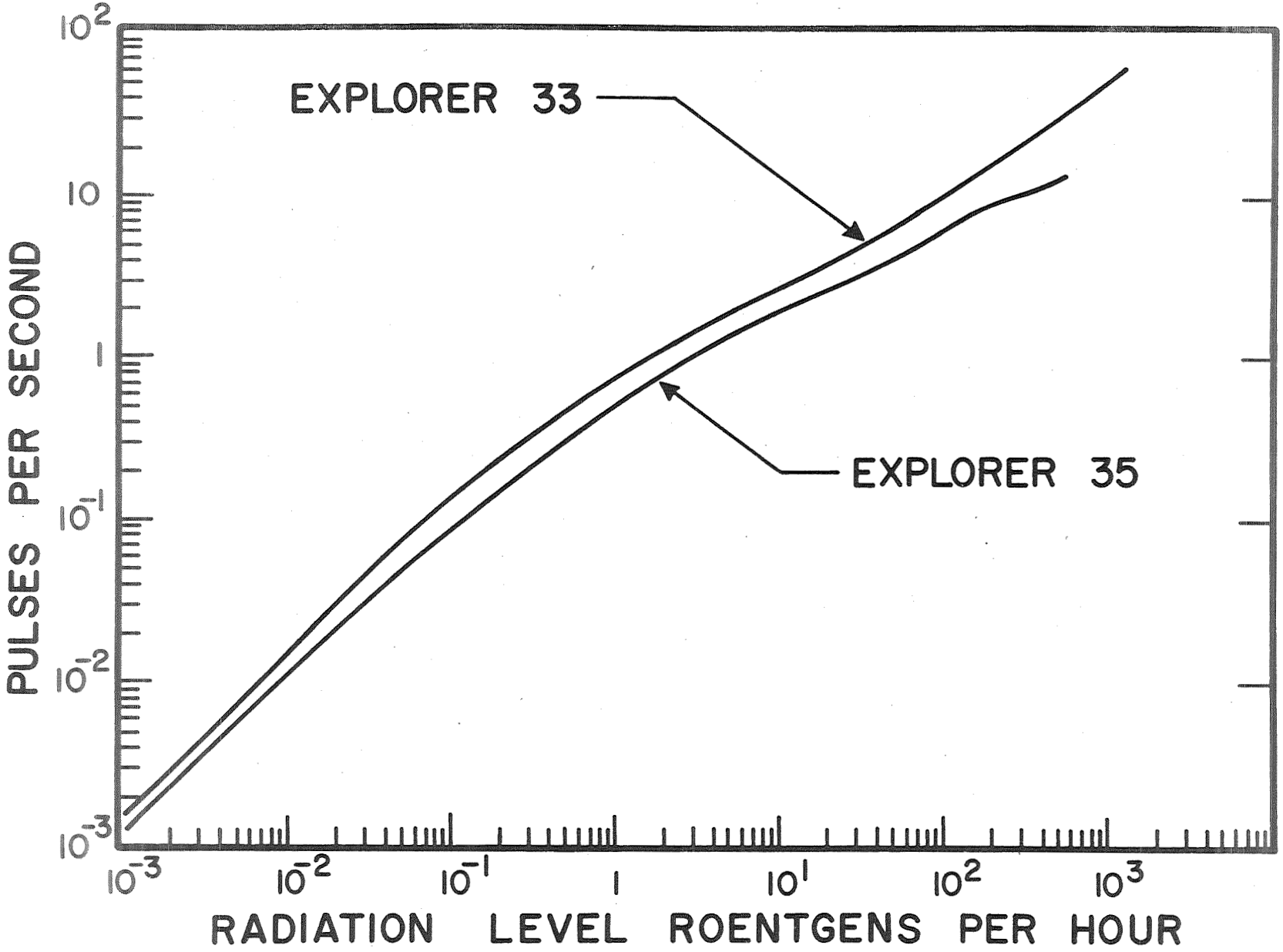
EXPLORER 33
EXPLORER 35
PULSES PER SECOND
10^2
10
1
10^{-1}
10^{-2}
10^{-3}
10^{-3}
10^{-2}
10^{-1}
1
10^1
10^2
10^3
RADIATION LEVEL ROENTGENS PER HOUR

Figure 7

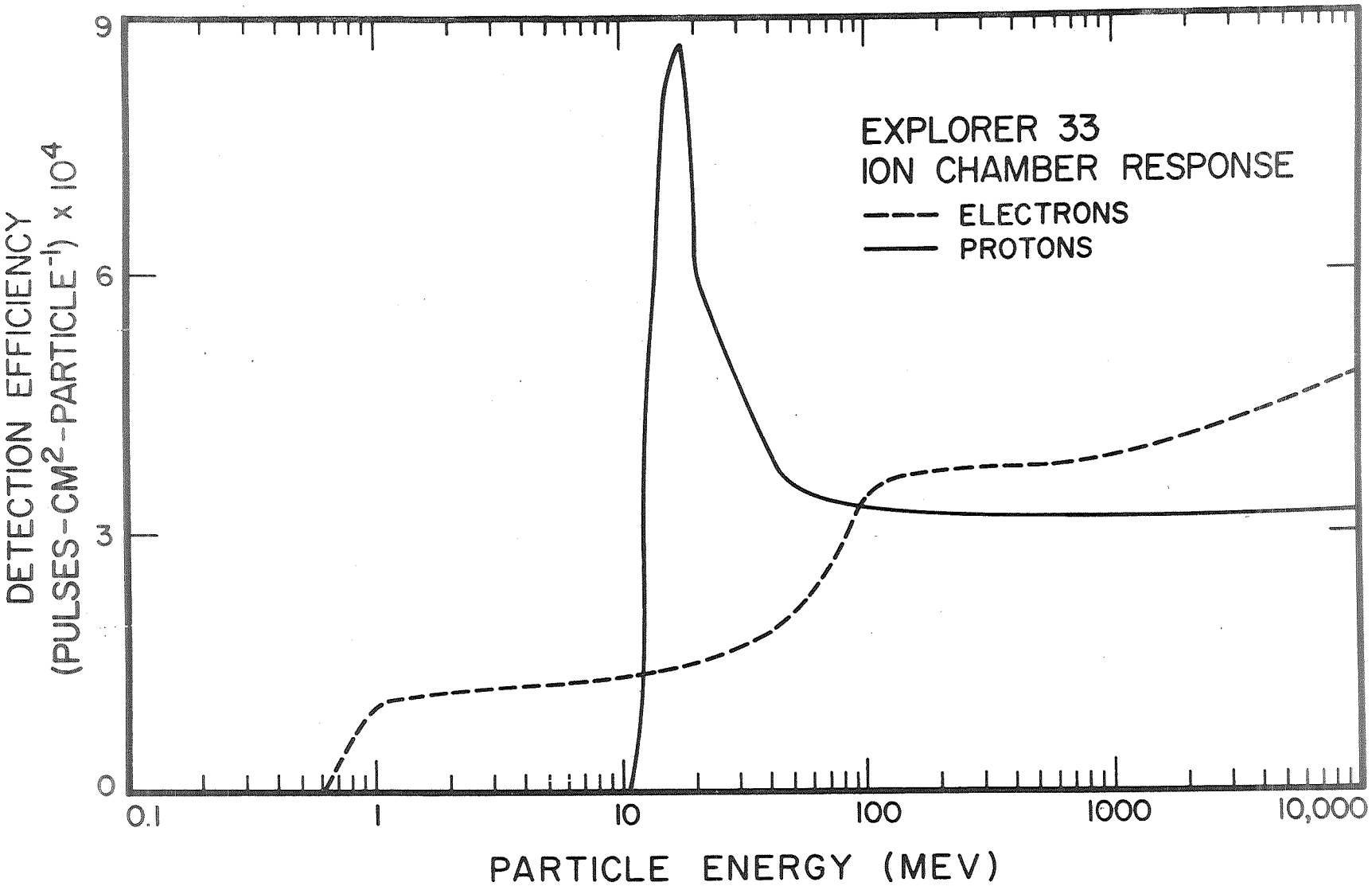
EXPLORER 33
ION CHAMBER RESPONSE
ELECTRONS
PROTONS
DETECTION EFFICIENCY
(PULSES-CM^2-PARTICLE^{-1}) x 10^4
9
6
3
0
0.1
1
10
100
1000
10,000
PARTICLE ENERGY (MEV)

Figure 8

are reset after readout. The experiment block diagram is given in Figure 9.

The two GM tubes feed accumulators directly after pulse shaping and amplification. These accumulators are the "S-T" type which will count signal pulses (S) up to the maximum of the accumulator (2^{15}-1) and will then count clock pulses (T) for the rest of the accumulation period.

The purpose of the "T" mode is to allow for an accurate interpretation of an overflow condition (where more pulses occur than can be counted during the accumulation time of a conventional, "S" mode counter). For each GM tube readout, a single 16-bit accumulator (either #5a and #6a) is used. If the 16th bit is "0" then the readout is the number of pulses acquired in the accumulation period. If the 16th bit is "1" then the first 15 bits of the accumulator give the number of clock pulses acquired after the overflow.

From Figure 10a, it can be seen that the last bit of the "S-T" accumulator is used for control to switch over and count the clock instead of signal inputs. The clock frequency selected (800 Hz) is such that the accumulator would not overflow if the clock were counted for the entire accumulation period. Therefore, as seen in Figure 10b the counting rate of the detector in the T mode is calculated by using the equation

$$\text{Rate} = \frac{2^{15}}{39.68 - T}$$

$$\text{where } T = \frac{T}{800}$$

and N is the count telemetered in the "T" mode.

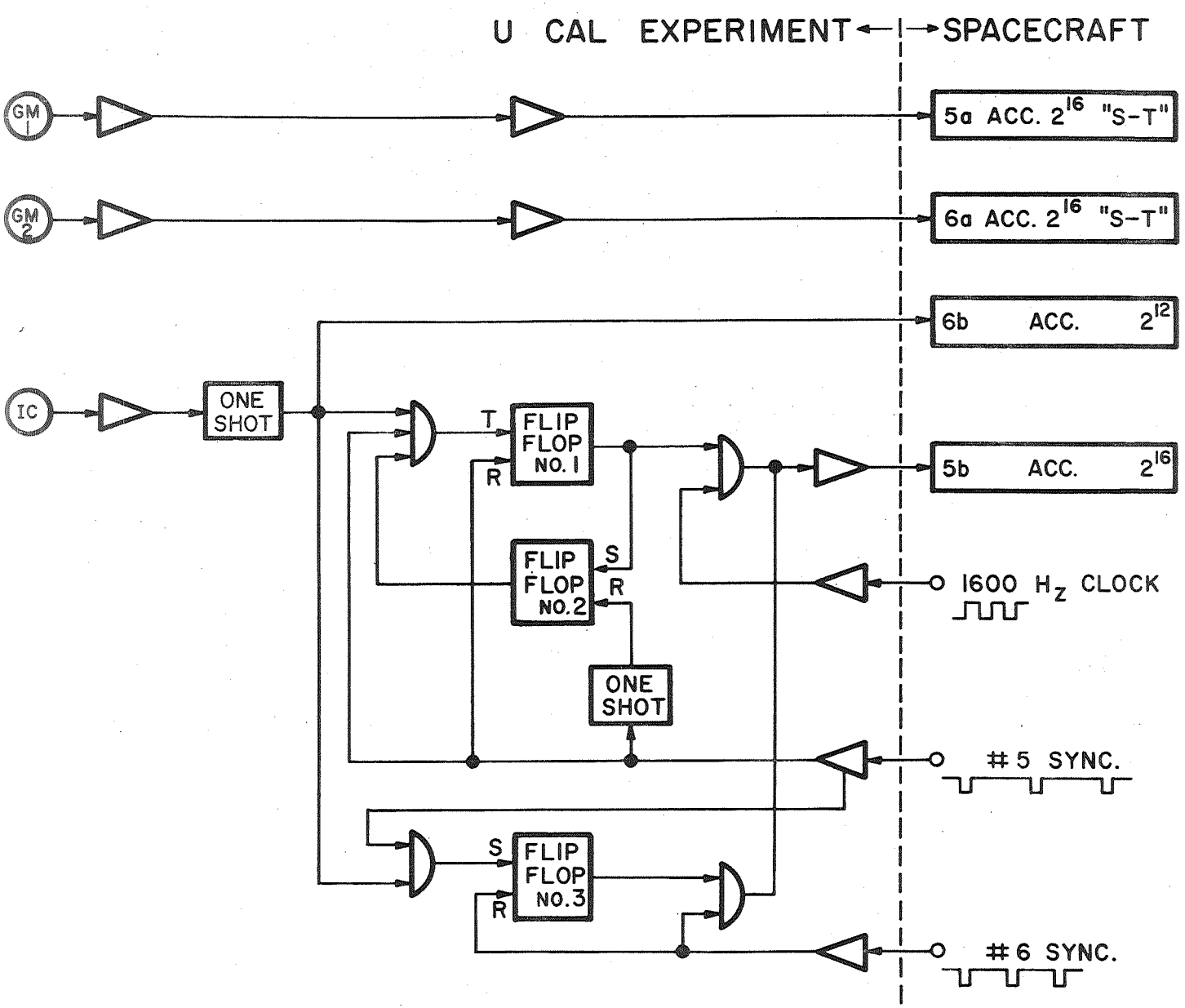
U CAL EXPERIMENT
SPACECRAFT
GM 1
GM 2
IC
ONE SHOT
T
R
FLIP FLOP NO. 1
FLIP FLOP NO. 2
S
R
ONE SHOT
S
R
FLIP FLOP NO. 3
5a ACC. 2^16 "S-T"
6a ACC. 2^16 "S-T"
6b ACC. 2^12
5b ACC. 2^16
1600 Hz CLOCK
#5 SYNC.
#6 SYNC.

Figure 9

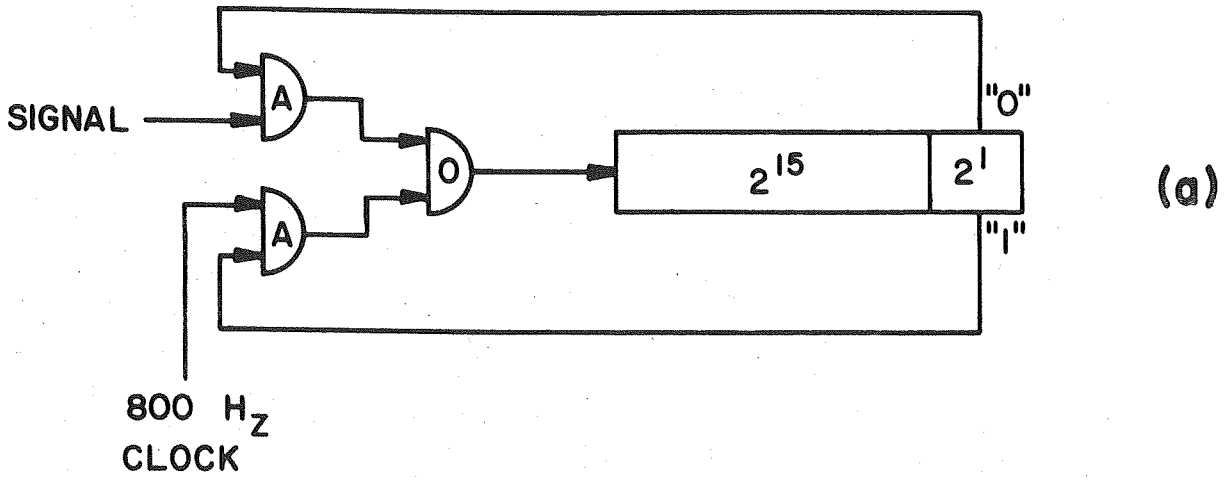
SIGNAL
A
A
O
2^{15}
2^{1}
"0"
"1"
800 H_Z
CLOCK

(a)

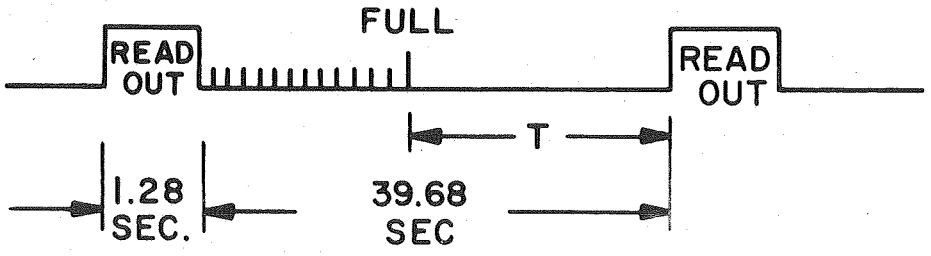
READ OUT
FULL
READ OUT
T
1.28 SEC.
39.68 SEC

(b)

Figure 10

For the ion chamber, one 12-bit and one 16-bit accumulator is used (#5b and #6b); one determines the total number of counts during the accumulation period while the other provides a measurement of the time period between ion chamber pulses. This method is used because of the typical low count rates and wide dynamic range of this detector (10^{-3} Hz to 10^{2} Hz).

The #6b accumulator is used to measure the total ion chamber counts per accumulation interval. The signal from the ion chamber is amplified and triggers a one-shot multivibrator which is used to drive the #6b accumulator circuits.

Accumulator #5b and the ion chamber logic circuits are used for the period measurements. A dual time-base technique is used -- the 1600 Hz clock and the 40.96 second repetitive time between the #5b accumulator readouts. (Refer to Figures 9 and 11.) The output of this accumulator can represent any of the following:

1. The elapsed time (T_1 or T_2) between the ion chamber pulse and the start of the #5b accumulator freeze time.
2. The elapsed time (T_3) between the first pair of ion chamber pulses occurring during the accumulation time of accumulator #5b.
3. The presence of an ion chamber pulse that occurred during the freeze time of the #5b accumulator, "hidden pulse."

Flip-flops #1 and #2 are reset at the beginning of the #5 accumulator freeze time and flip-flop #3 is reset at the end of the #6 accumulator freeze time. The ion chamber output, after shaping by the one-shot multivibrator, triggers flip-flop #1 which gates the 1600 Hz

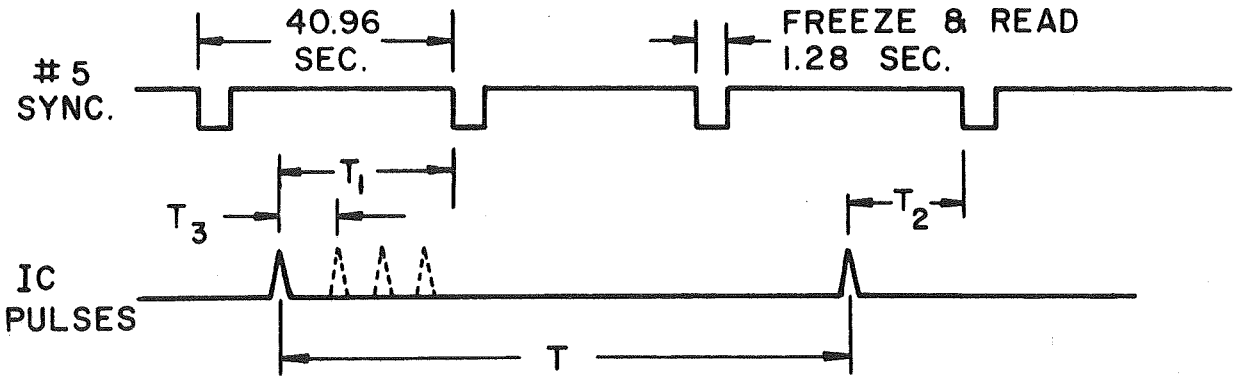

Figure 11

clock into the #5b accumulator. If there are no other ion chamber outputs before the accumulation period ends, then the clock count is stopped by resetting flip-flop #2 with the #5 sync (accumulator freeze). The stored count in the accumulator then represents T_1 (or T_2). This same process is repeated each time there is only one ion chamber pulse per accumulation period. Thus, by knowing T_1, T_2 and the number of no pulse readouts that have occurred between them, the period T of an ion chamber pulse pair can then be calculated.

If a second IC pulse occurs during the accumulation time of #5b, then this pulse will toggle flip-flop #1 back to its original state, and thus block further clock pulses from reaching the #5b accumulator. This action of flip-flop #1 will also set flip-flop #2 and prevent any further toggle pulses from reaching flip-flop #1. Thus, the count contained in the #5b accumulator will then represent the time T_3 -- that is, the period between the first pair of pulses occurring in the accumulation interval.

Since there is a probability of an ion chamber pulse occurring during the freeze and readout time for the #5b accumulator ("hidden pulse") and since this could be significant for period measurement at the low count rates, a means is provided to identify the occurrence of these pulses. Flip-flop #3 and the two associated gates are used for this purpose (Figure 9). If an IC pulse occurs during the #5 freeze time it is sensed in a logic gate and used to set flip-flop #3. Flip-flop #3 then serves as a memory and this condition is then readout during the #6 freeze time via a gate and passed into the accumulator #5b to register as a single count. Thus, when the IC period, "T," is greater than 39.68 seconds these "hidden pulses" are identifiable

by a single count in the #5b accumulator -- with IC periods less than 39.68 seconds this single count could be covered up by 1600 Hz clock pulses.

The general equation for computing the ion chamber period, T, when a single (and no pulse) occur during the #5b accumulation time can be given as,

$$T = \frac{(N_Z + 1)\ 40.96 + (N_1 - N_2)/1600}{N + 1}$$

where T = the IC period in seconds

N_2 = the present #5b readout (accumulated counts)

N_1 = the last #5b readout > 1 preceeding the N_2 readout

N_Z = the number of #5b readouts which have been 0's or 1's between the N_1 and N_2 readouts

N = the number of #5b readouts which have been 1's between the N_1 and N_2 readouts.

When 2 or more pulses occur during the #5b accumulation time the period, T, for the pulse pair is

$$T = \frac{N_p}{1600}$$

where N_p = the accumulation count in #5b.

Telemetry

The University of California experiment uses three 16-bit accumulators and one 12-bit accumulator in the Digital Data Processor (DDP) section of the spacecraft Encoder. Each accumulator is read out and

reset twice every spacecraft sequence. An additional 4 bits are used for a redundancy check on the #6a accumulator.

Figure 12 shows the relative timing for each of the 4 outputs from the experiment. The freeze and readout of accumulators #5a and #5b occurs at the same time. (This is also true for #6a and #6b.) The #5 accumulator readouts lead the #6 accumulators readouts by 2.56 seconds.

The telemetry format positions for one sequence are indicated in Figure 13. During each channel, two 4-bit (hexadecimal) bursts are transmitted. The 4 most significant bits of accumulator #6a are re-transmitted as indicated in Figure 14 -- bit 1 is the least significant bit.

Explorer-33 Experiment History

All detectors operated normally from launch on June 30, 1967 until August 1, 1967. On August 1, GM2 of Explorer-33 began to behave erratically. At this time it was counting an average 3000 counts per second from solar x-rays. By August 4, the count rate of GM2 had risen to 10,000 counts per second, which was higher than the saturation rate achieved in laboratory tests. On August 9, GM2 stopped counting and a few days later GM1 also stopped. Studies in the laboratory on similar tubes indicated that GM2 had apparently gone into a neon lamp type discharge, and drawn enough current to lower the power supply voltage below the starting potential of GM1. This malfunction may have been due to two causes:

1. loss of some gas from the counter, due to a pinhole leak in the very thin window of the counter, or a leak elsewhere in the counter walls; or

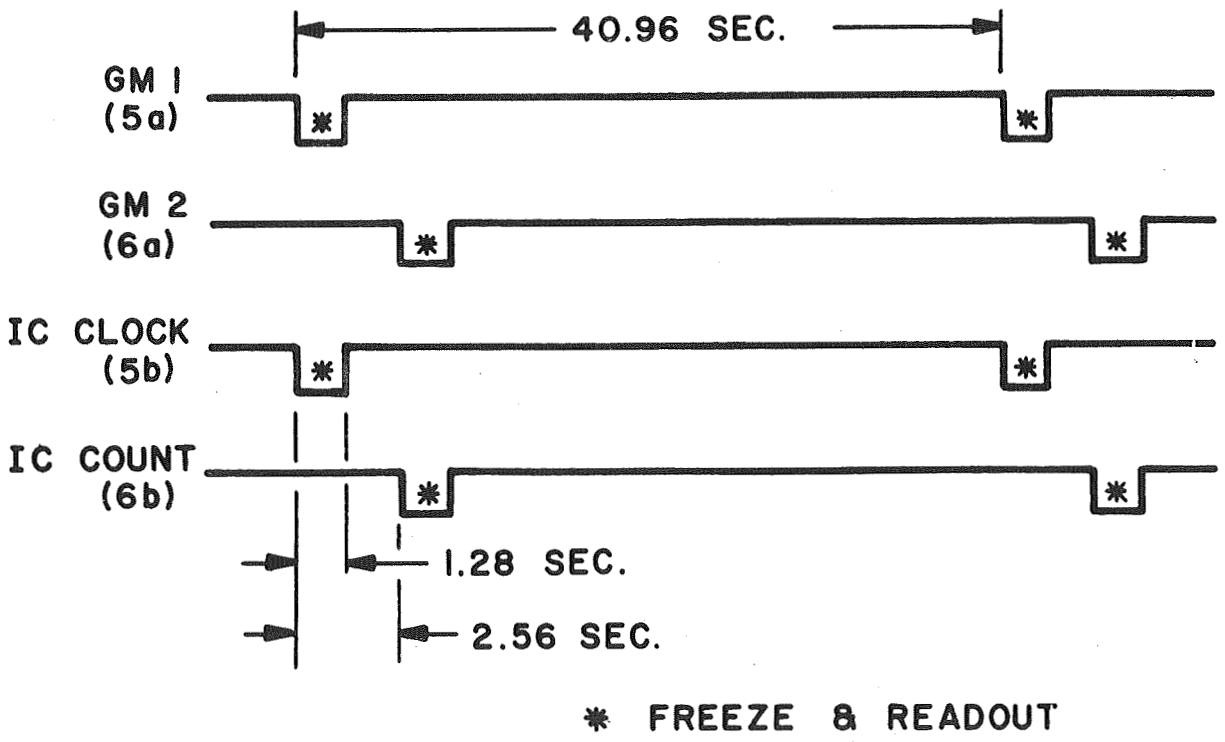
40.96 SEC.
GM 1
(5a)
GM 2
(6a)
IC CLOCK
(5b)
IC COUNT
(6b)
1.28 SEC.
2.56 SEC.
* FREEZE & READOUT

Figure 12

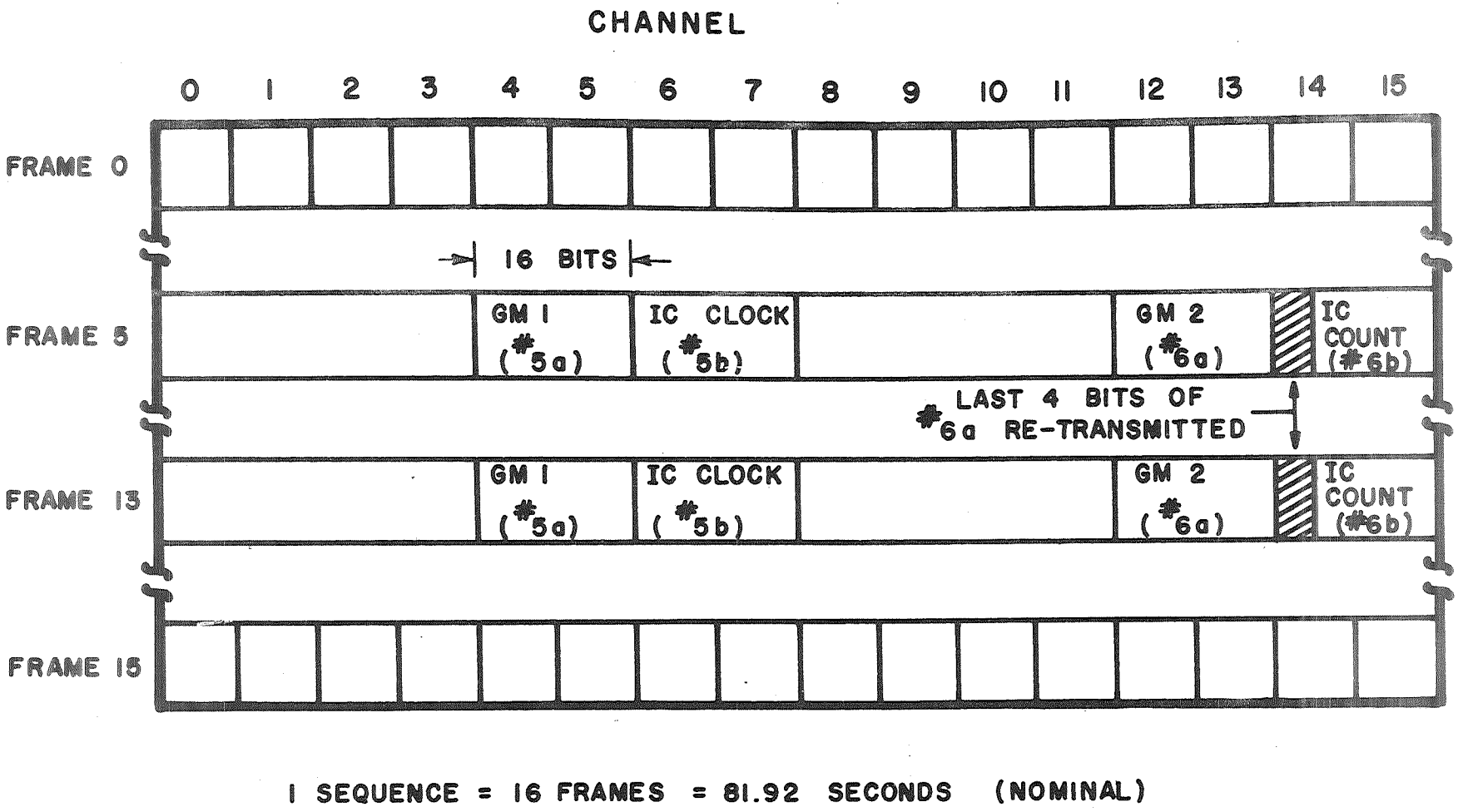

1 SEQUENCE = 16 FRAMES = 81.92 SECONDS (NOMINAL)

Figure 13

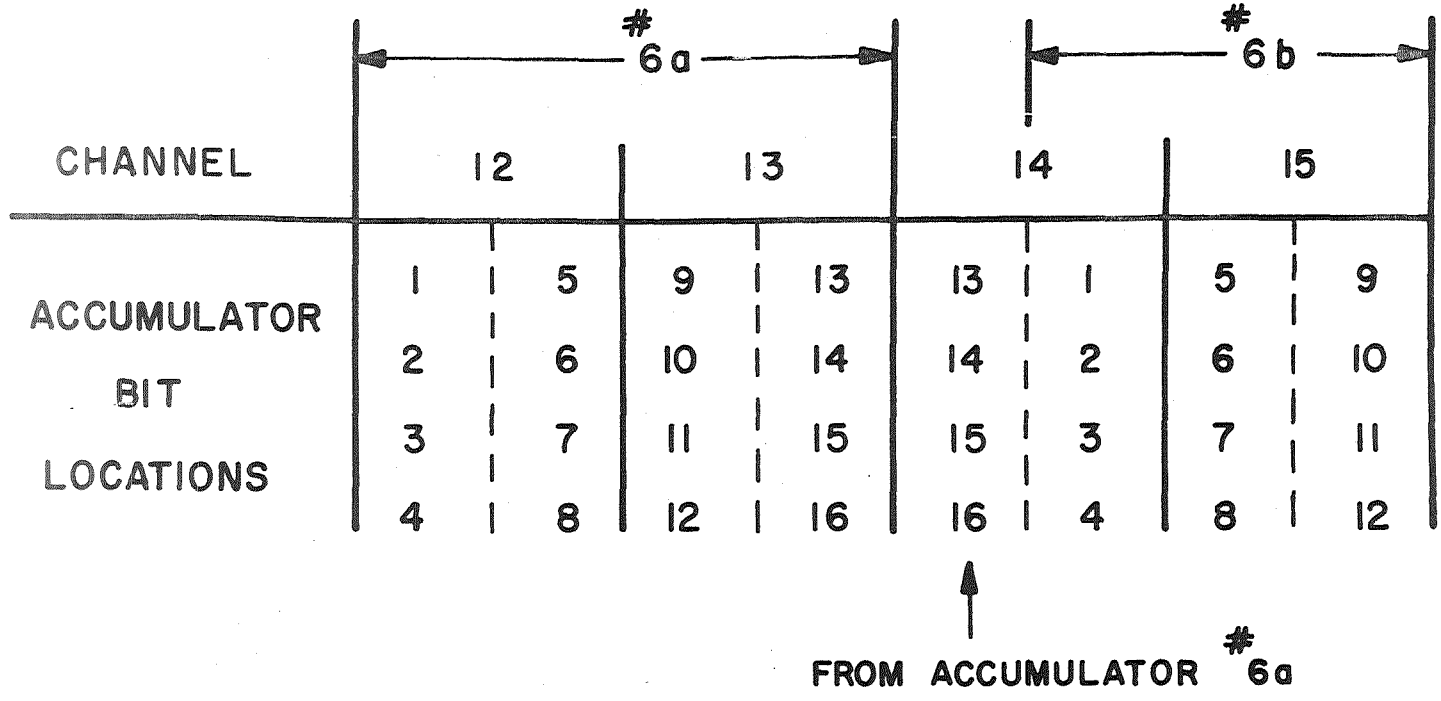
#6a
#6b
CHANNEL
12
13
14
15
ACCUMULATOR BIT LOCATIONS
1 5 9 13 13 1 5 9
2 6 10 14 14 2 6 10
3 7 11 15 15 3 7 11
4 8 12 16 16 4 8 12
FROM ACCUMULATOR #6a

Figure 14

2. absorption of the quenching gas on the walls of the counter from the catalytic action of the large x-ray flux.

On September 2, 1966 the current drawn by GM2 became sufficiently large to lower the supply voltage and stop GM1 also. The ion chamber with a lower voltage threshold of 350V continued to operate until October 20, 1967. No usable data was obtained after that date.

Explorer-35 Experiment History

All detectors operated normally from launch on July 19, 1967 until November 17, 1967. At that time detector GM2 began exhibiting occasional spikes in its counting rate which may be due to either partial breakdown of the quenching gas or a malfunction in the accumulator. In this regard it is noted that the occurrence of the spikes was count rate dependent, occurring more often at higher counting rates. Also the interval between spikes appeared to be somewhat regular. The data remained quite completely usable since these spikes were fairly constant in counting rates and therefore never confused real events. On November 19, 1968 after a particularly intense solar event the ionization chamber failed. We believe the tungsten filament welded itself onto the anode of the chamber. On May 9, 1969, the GM2 (open detector) ceased to count following an intense solar event in April. Prior to the termination of counting, GM2 exhibited a continuous discharge mode, counting $\geq 10^4$ counts/sec, probably due to the loss of the quench gas. GM1 continued counting and as of May 14, 1970 was still operating normally.

REFERENCES

1. Trower, W.P., High Energy Particle Data, Volume II. Range-Energy and dE/dX Plots of Charged Particles in Matter, University of California, Lawrence Radiation Laboratory, Berkeley, Publication UCRL-2426, 1966

2. Fermi, E., Notes compiled by J. Orear, A.H. Rosenfeld, and R.A. Schluter, Nuclear Physics, University of Chicago Press, Chicago, Illinois, p. 36, 1950

3. Anderson, K.A., H.K. Harris and R.J. Paoli, J. Geophys. Res., 70, 1039, 1965

4. Siegbahn, K., Alpha-, Beta- and Gamma-Ray Spectroscopy, V1, N. Holland Publishing Co., Amsterdam, Netherlands, 1965

II. DESCRIPTION OF THE DATA FORMAT ON MAGNETIC TAPES SUPPLIED TO THE NATIONAL SPACE SCIENCE DATA CENTER

The magnetic tapes submitted to the National Space Science Data Center contain all the data from the University of California experiments on the AIMP-1 and -2 spacecraft. Each tape is generated by stacking seven short data tapes received from Goddard Space Flight Center on a 2400 foot reel. The stacked tapes were written on an IBM 360/40 system. They contain external BCD characters written in 7 track mode in even parity at 800 char/in density.

The first file on each stacked tape is a one record file which serves as an index to that tape. The physical record (gap to gap) is 865 characters long and can contain 72 twelve character logical records. There is one index entry for each of the seven GSFC short reels stacked on the larger tape. The remaining 65 entries are not used. The entries are in the following format:

Chars	
1-6	GSFC reel number
7-9	Number of files contained on the GSFC tape
10-12	Blank

Following the index file is the stacked experiment data copied from the GSFC reels. The data is in the same file by file format as it appeared on the original tapes except that a 12-character field has been prefixed to each record to identify it to UC programs using these tapes. The individual records are 865 characters (including prefix field) and are formatted as follows:

Chars	
1-6	The GSFC reel number on which this record originally appeared
7-9	The file number within that GSFC reel
10-12	The record number within the above file
13-864	The experimental data in its original format (see "AIMP Stacked Data Tape Format" below).

The last file on each of the GSFC tapes is a one record file with the twelve character identification field (i.e., Satellite No., Month, Day, etc.) set to nines. This file has also been copied onto the stacked tape. Thus the first record of the following file on the stacked tape will have a different GSFC reel number and a file number of 1 in the prefix field. Two end-of-file marks will follow the last valid data file on the stacked tape. Figure 15 shows the tape structure.

AIMP Stacked Data Tape Format

Item	Significance	Tape Chars	
P1	Original GSFC reel number	6	
P2	File number within GSFC reel	3	Prefix fields
P3	Record number within above file	3	
1	Identification (ID)		
	(a) Satellite	2	
	(b) Julian Day of Year	3	ID fields
	(c) Year	2	
	(d) Data Acquisition Station	2	
	(e) Analog Tape Number	3	

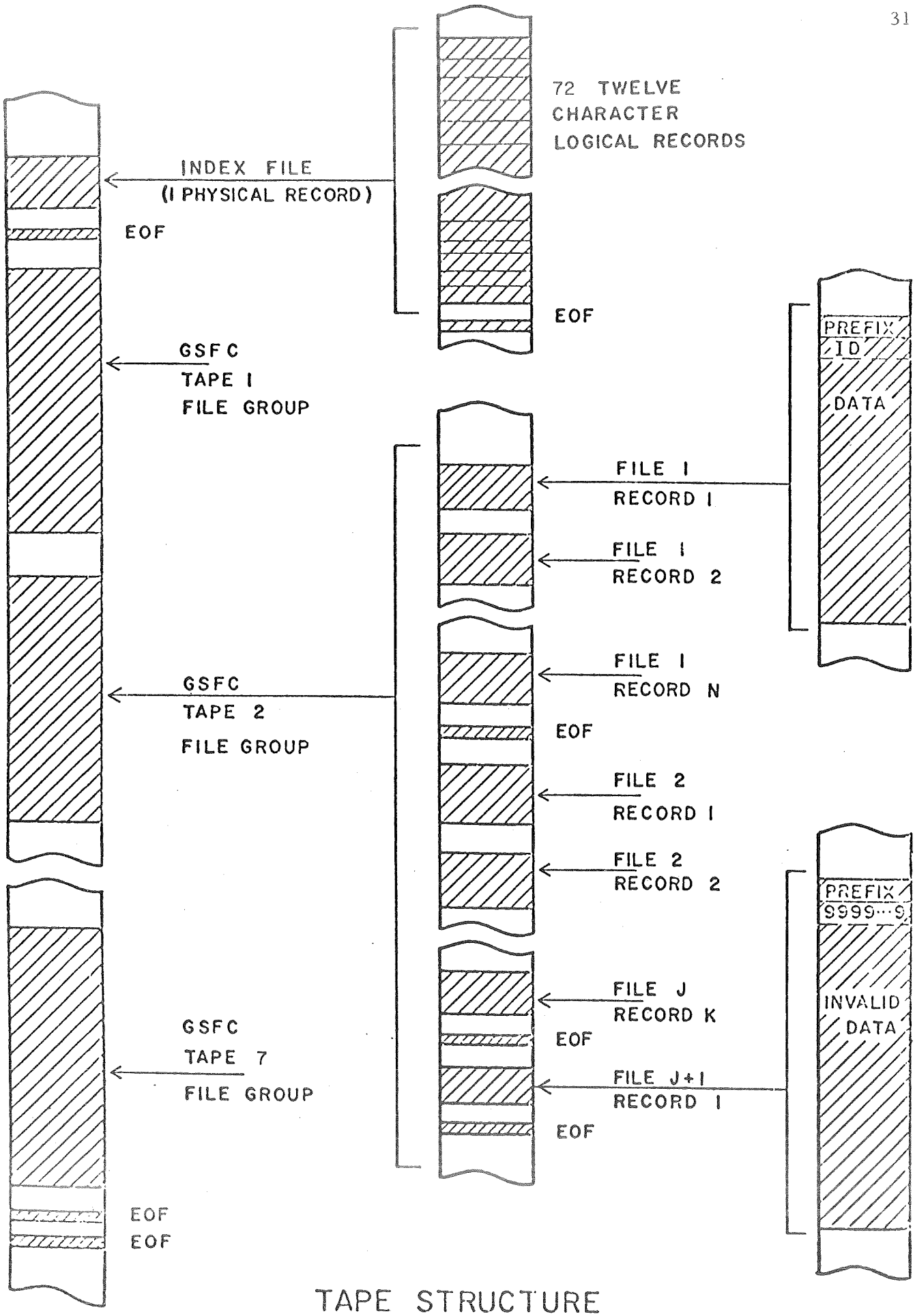

TAPE STRUCTURE

Figure 15

Item	Significance	Tape Chars	
2	A/D Line Indicator	1	
3	Time for the Middle of Channel Ø, Frame Ø		
	(a) Day Count of Year (Jan. 1 = 0)	3	
	(b) Fractional Day of Year (Millisecond Precision)	8	
	(c) Blank	1	
4	Time Flag	2	
5	Sequence Counter ("Satellite Clock") (1 Decimal Number)	6	
6	Frame Rate	4	
7	Sequence Identification	1	
Items 8 through 23 repeated two (2) times per sequence, i.e., for frames 5 and 13.			
8	Frame Number	2	Data fields
9	Pre Data Flag	1	
10	Raw Data (4 Comb Filter Numbers)	12	
11	Guardband Flag	1	
12	Converted Data (1 Decimal Number of max. 65,535) (GM1)	5	
13	Raw Data (4 Comb Filter Numbers)	12	
14	Guardband Flag	1	
15	Converted Data (1 Decimal Number of max. 65,535) (IC Clock)	5	
16	Raw Data (4 Comb Filter Numbers)	12	
17	Guardband Flag	1	
18	Converted Data (1 Decimal Number of max. 65,535) (GM2)	5	
19	Raw Data (1 Comb Filter Number)	3	
20	Raw Data (3 Comb Filter Numbers) (IC Redundant)	9	
21	Guardband Flag	1	
22	Converted Data (1 Decimal Number of max. 4095) (IC Count)	4	
23	Post Data Flag	1	
24	Data Quality Flag	1	
25	Performance Parameter (1 Decimal Number of max. 255)	3	

Item	Significance	Tape Chars
26	Performance Parameter (1 Decimal No. of Max. 255)	3
27	Performance Parameter (1 Decimal No. of Max. 255)*	3
28	Optical Aspect	
	(a) Pseudo Sun Pulse Flag	2
	(b) Sun Angle (1 Octal No. of Max. 7778)	3
	(c) Spin Period (1 Decimal No. of Max. 4095)	4
	(d) Sun Time (1 Decimal No. of Max. 4095)	4
	(e) Moon Time 1 (1 Decimal No. of Max. 4095)	4
	(f) Moon Time 2 (1 Decimal No. of Max. 4095)	4
	(g) Moon Time 3 (1 Decimal No. of Max. 4095)	4
	TOTAL NUMBER OF CHARACTERS PER SEQUENCE	223

Four of the above described sequences are blocked together with the exception that the last three (3) sequences of the block do not contain the prefix fields (Items P1, P2, P3) and the Identification (ITEM #1) or A/D Line Indicator (ITEM #2) to make a total of 865 BCD characters per block.

NOTE 1: Fill data for items 12, 15, 18, 22 is indicated by 9's throughout the field.

NOTE 2: Optical Aspect and Performance Parameters tables will be made available to investigators upon request.

*In a Sequence 1 Item #25 will be PP1, Item #26 will be PP2, Item #27 will be PP7.

In a Sequence 2 Item #25 will be PP14, Item #26 will be PP15, Item #27 will be PP16.

In a Sequence 3 Item #25 will be PP17, Item #26 will be PP18, Item #27 will be PP19.

In a Sequence 4 Item #25 will be PP20, Item #26 will be PP22, Item #27 will be PP24.

NOTE 3: Rate Calculations

A. GM1 and GM2 rates

1. "S" Mode

if N < 32768 ("T" Bit = Ø)

$$R_o = \frac{N}{39.680\ K}$$

2. "T" Mode

if N > 32768 ("T" Bit = 1) Then N = N - 32768

and

$$R_o = \frac{32768}{[39.680 - (N/800)]\ K}$$

R_o: GM1 (or GM2) rate in pulses per second.

N: The GM1 (or GM2) accumulator value -- 15 least significant bits.

K: Time base correction factor

$$K = \frac{FR}{NFR} = \frac{FR}{5926}$$

FR: Actual frame rate from data.

NFR: Nominal frame rate in fractional part of a day.

$$NFR = \frac{5.12\ sec}{60 \times 60 \times 24} = 0.00005926\ day$$

B. Ion Chamber rate calculations

1. ICCLK rate -- Interval method

a. Equations

(1) $$R_i = \frac{N_o + 1}{(N_z + 1)\ 40.96K + (N_1 - N_2/1600K)}$$

(2) $$R_i = \frac{1600K}{N_2}$$

R_i: The ion chamber rate in pulses per second.

N_1: The last ICCLK value 1 preceding the present value.

N_2: The present ICCLK value 1

N_o: The number of ICCLK values that have been 1's between the N_1 and N_2 values.

N_z: The number of ICCLK values which have been o's or 1's between the N_1 and N_2 values.

K: The time base correction factor (see part A of Note 3).

b. Conditions for use of interval method: use equation (1) if two pairs of values exist such that ICCLK > 1 and ICCNT = 0 or 1
Use equation (2) if ICCLK > 1 and ICCNT ≥ 2.
If none of the above conditions exist, then the interval method cannot be applied.

c. Notes for interval method.

1) The sequence count is used to determine N_z.

2) If either a "gap" or "invalid data" occur between N_1 and N_2 then an ICCLK value of 0 may be assumed for that readout or readouts.

"gap": One (1) or more missing sequence of data.

"invalid data": Non-numeric ICCLK value or ICCLK value of all 9's.

3) Each tape file is to be considered as an independent set of ICCLK and ICCNT values for the interval calculations.

2. ICCNT rate -- Count method

If ICCNT > 10

$$R_c = \frac{N_c}{39.680K}$$

otherwise the count rate is not computed and is left blank in the print-out.

R_c: ICCNT rate in pulses per second.

N_c: ICCNT accumulator value (on tape).

K: The time correction factor (see part A of Note 3).

III. AIMP-1, 2 MAJOR COMPUTER PROCESSING PROGRAMS

The following is a brief description of the major computer programs used to process the University of California AIMP-1, 2 satellite data:

1. AIMP-RATE

   The AIMP-RATE program serves as the primary "raw" printout on a production basis for AIMP data. About one-half of the printout is dumped from the tape. The remaining printout is the result of rate calculations for the three experiment detectors, performance parameter calculations, and other miscellaneous items.

   The program was written by Barbara Watson for the IBM 7094 in July, 1966.

2. PLOT24

   The PLOT24 program produces a one-inch/hour five cycle semi-log plot of the two GM outputs and the ion chamber. This plot serves as the primary display of the AIMP experimental data.

   The program was completed by Maria Roberts for the IBM 7094 in October, 1966 and later modified for the CDC 6400 in July, 1967.

3. LSEP

   LSEP is the program used to process AIMP orbit trajectory tapes on a production basis. It calculates and lists orbit trajectory parameters relevant to the University of California experiments. Two alternate versions exist. IELSEP lists parameters relevant to the lunar orbit of AIMP-2. AILSEP lists parameters relevant to the earth orbit of AIMP-1.

The program was written by Barbara Watson for the IBM 7094 in July, 1967 and later modified for the CDC 6400 by G. Pitt.

4. AIMP-OTPLT

This program plots values of satellite distance in R_e and LSEP and MLAT in degrees for a 24-hour period. The input is from AIMP orbit trajectory tapes. The time axis is 24 inches long and corresponds with the 1-inch/hour data plots.

The program was written by Barbara Watson and George Pitt in August, 1966 for the IBM 7094. It was later modified for the CDC 6400.

5. AIMP-AVRATE

This program calculates corrected rates and average corrected rates for the AIMP GM detectors, observed count and clock rates for the Ion chamber and calculates various spectrum parameters.

The program was written by George Pitt in August, 1966 for the IBM 7094 and later modified for the CDC 6400.

6. AIMP STACK SYSTEM

The AIMP STACK SYSTEM is an integrated system of programs designed to maintain AIMP satellite data tapes in convenient, compact form and facilitate the manipulation of individual data tapes.

The programs were written in July, 1966 by Maria Roberts for the IBM 360/30.

IV. LIST OF PUBLICATIONS REPORTING RESULTS FROM THE EXPLORER 33 & 35 SATELLITES

1. Observations of solar flare electrons in interplnaetary space, R.P. Lin, PHD Dissertation, Physics Department, University of California, Berkeley, August, 1967

2. Correlations of solar-flare electron events with radio and x-ray emission from the sun, R. P. Lin, Canad. J. Phys. 46, 5757, 1968

3. Observations of bow shock and upstream energetic electron spikes, K.A. Anderson, Book of Summaries and Abstracts, International Symposium on Physics of the Magnetosphere, Washington, D.C., 1968

4. Observations of lunar shadowing of energetic particles, R.P. Lin, J. Geophys. Res. 73, 3066, 1968

5. Solar flare injection and propagation of low-energy protons and electrons in the event of 7-9 July 1966, R.P. Lin, S.W. Kahler and E.C. Roelof, Solar Phys. 4, 338, 1968

6. Observation of interplanetary field lines in the magnetotail, K.A. Anderson and R.P. Lin, J. Geophys. Res. 74, 3953, 1969

7. Electrons and protons in long-lived streams of energetic solar particles, K.A. Anderson, Solar Phys. 6, 111, 1969

8. Energetic electrons of terrestrial origin behind the bow shock and upstream in the solar wind, K.A. Anderson, J. Geophys. Res. 74, 95, 1969

9. Relation of energetic particles in the plasma sheet to the auroral zone, K.A. Anderson, Atmospheric Emissions, ed. by B.M. McCormac and Anders Omholt, Van Nostrand Reinhold Pub. Co., 327, 1969

10. The solar particle event of July 16-19, 1966 and its possible association with a flare on the invisible solar hemisphere, H.D. Prince, E.R. Hedeman, S.W. Kahler and R.P. Lin, Solar Phys. 6, 294, 1969

11. Spatial gradients of energetic protons and electrons observed after the 7 July 1966 solar flare, S.W. Kahler and R.P. Lin, Annals of the IQSY, Vol. 3, The Proton Flare Project (The July 1966 Event), M.I.T. Press, Cambridge, Mass., 299-312, 1969

12. Method to determine sense and magnitude of electric field from lunar particle shadows, K.A. Anderson, J. Geophys. Res. 75, 2591, 1970

13. Observations of scatter-free propagation of ~40 KeV solar electrons in the interplanetary medium, R.P. Lin, J. Geophys. Res. 75, 2583, 1970

14. The emission and propagation of ~40 KeV solar flare electrons, I. Relationship of ~40 KeV electron to energetic proton and relativistic electron emission by the sun, R.P. Lin, Solar Phys. 12, 266, 1970

15. A layer of energetic electrons (> 40 keV) near the magnetopause, C.I. Meng and K.A. Anderson, J. Geophys. Res. 75, 1827, 1970

16. The emission and propagation of ~40 keV solar electrons, R.P. Lin, Acta Physica Academiae Scientiarum Hungaricae 29, Supp. 2, 669, 1970

17. Solar and galactic cosmic rays and the interplanetary magnetic field 28 January-25 February 1967, S.T. Lindgren, Acta Physica Academiae Scientiarum Hungaricae 29, Supp. 2, 1970

18. The emission and propagation of ~40 keV solar flare electrons, II. The electron emission structure of large active regions, R.P. Lin, Solar Phys., in press

19. Energetic electrons in the magnetotail at 60 R_e, C.I. Meng, J. Geophys. Res., in press

20. A theoretical treatment of lunar particle shadows (Part I), R.E. McGuire, to be submitted to Cosmical Electrodynamics

21. The acceleration and emission of 10-100 keV electrons by solar flares, H.S. Hudson and R.P. Lin, in preparation

V. PAPERS PRESENTED AT SCIENTIFIC MEETINGS REPORTING RESULTS FROM THE EXPLORER 33 & 35 SATELLITES

1. Observations of solar flare electrons, R. P. Lin, Tenth International Conference on Cosmic Rays, Calgary, Canada, 1967

2. Problems connected with solar particle events -- particle physics, K.A. Anderson, ESLAB/ESRIN Symposium, Noordwijk, Holland, 1967

3. Preliminary results of the energetic particle experiment on Explorer 33, R.P. Lin, R.J. Paoli and K.A. Anderson, American Geophysical Union Annual Meeting, Washington, D.C., 1967 (in Trans. AGU 48, 160, 1967)

4. Solar electron events 1964-1967, R.P. Lin and K.A. Anderson, Midwest Cosmic Ray Conference, Iowa City, Iowa, 1968

5. The solar particle events of May 23 and May 28, 1967, S.T. Lindgren, Midwest Cosmic Ray Conference, Iowa City, Iowa 1968

6. Energetic electrons of terrestrial origin at 60 R_e geocentric distance, K.A. Anderson, American Geophysical Union Annual Meeting, Washington, D.C., 1968 (in Trans. AGU 49(1), 1968)

7. Effects of the moon on energetic solar protons and electrons, R. P. Lin, American Geophysical Union Annual Meeting, Washington, D.C., 1968 (in Trans. AGU 49(1), 1968)

8. Lunar shadowing of solar and terrestrial electron fluxes, R.P. Lin, American Geophysical Union National Fall Meeting, San Francisco, California, 1968 (in Trans. AGU 49(4), 1968)

9. Observations of 3- to 10-MeV protons in energetic storm particle events, S.W. Kahler, American Geophysical Union Annual Meeting, Washington, D.C., 1968 (in Trans. AGU 49(4), 1968)

10. The recurrent proton events of June 24 and September 27, 1966, S.W. Kahler, AAS Special Meeting on Solar Astronomy, Tucson, Arizona, 1968

11. Electrons from solar flares, K.A. Anderson, American Physical Society Meeting, Miami, Florida, 1968

12. Electrons and protons in long-lived streams of energetic solar particles, K.A. Anderson, AAS Special Meeting on Solar Astronomy, Pasadena, California, 1969

13. Entry of solar cosmic rays into the earth's magnetosphere, K.A. Anderson, Summer Advanced Study Institute, Earth's Particles and Fields, Santa Barbara, California, 1969

Papers Presented at Scientific Meetings Reporting Explorer 33 & 35 Results
Page 2

14. Energetic electrons at the magnetopause, C.I. Meng, Summer Advanced Study Institute, Earth's Particles and Fields, Santa Barbara, California, 1969

15. Solar particles and related solar phenomena, K.A. Anderson, XI International Conference on Cosmic Rays, Budapest, Hungary, 1969

16. High energy particles in the earth's magnetotail, K.A. Anderson, IAGA Meeting, Madrid, Spain, 1969

17. Energetic particles in the magnetotail, K.A. Anderson, American Geophysical Union Annual Meeting, Washington, D.C., 1969 (in Trans. AGU 50(4), 1969)

18. The earth's magnetosphere, K.A. Anderson, Sixteenth Annual West Coast Research Reserve Seminar, Treasure Island, San Francisco, California, 1969

19. Particle shadowing by the moon, K.A. Anderson and R.P. Lin, American Geophysical Union Annual Meeting, Washington, D.C., 1969 (in Trans. AGU 50(4), 1969)

20. Simultaneous x-ray and electron emission from the sun, H.S. Hudson and R.P. Lin, AAS Special Meeting on Solar Astronomy, Pasadena, California, 1969

21. Halo structure of solar proton events, S.W. Kahler, R.P. Lin and E.C. Roelof, AAS Special Meeting on Solar Astronomy, Pasadena, California, 1969

22. Fluxes of ~40 keV electrons associated with solar active regions, R.P. Lin, American Geophysical Union Annual Meeting, Washington, D.C., 1969 (in Trans. AGU 50(4), 1969)

23. The emission of ~40 keV electrons by the sun, R.P. Lin, AAS Special Meeting on Solar Astronomy, Pasadena, California, 1969

24. Coronal storage and interplanetary propagation of low energy solar particles, E.C. Roelof and R.P. Lin, American Geophysical Union National Fall Meeting, San Francisco, California, 1969 (in Trans. AGU 50(11), 667, 1969)

25. A layer of energetic electrons (> 40 keV) near the magnetopause, C.I. Meng, American Geophysical Union Annual Meeting, Washington, D.C., 1970 (in Trans. AGU 51, 1970)

26. The emission and propagation of ~40 keV solar electrons, R.P. Lin, XI International Conference on Cosmic Rays, Budapest, 1969

Papers Presented at Scientific Meetings Reporting Explorer 33 & 35 Results
Page 3

27. Solar and galactic cosmic rays and the interplanetary magnetic field 28 January-25 February 1967, S.T. Lindgren, Eleventh International Conference on Cosmic Rays, Budapest, 1969

28. Fluxes of ~40 keV electrons associated with solar active regions, R.P. Lin, International Symposium on Solar-Terrestrial Physics, Leningrad, USSR, 1970